Noname manuscript No.
(will be inserted by the editor)

Thermography data fusion and non-negative matrix factorization for the evaluation of Cultural heritage objects and buildings

Bardia Yousefi · Stefano Sfarra · Clemente Ibarra-Castanedo · Nicolas P. Avdelidis · Xavier P. V. Maldague ·

Received: date / Accepted: date

Abstract The application of the thermal and infrared technology in different areas of research is considerably increasing. These applications involve Non-destructive Testing (NDT), Medical analysis (Computer Aid Diagnosis/Detection-CAD), and Arts and Archeology among many others. In the arts and archaeology field, infrared technology provides significant contributions in term of finding defects of possible impaired regions. This has been done through a wide range of different thermographic experiments and infrared methods. The proposed approach here focuses on application of some known factor analysis methods such as standard Non-Negative Matrix Factorization (NMF) optimized by gradient-descent-based multiplicative rules

B. Yousefi, C. I. Castanedo, X. P. V. Maldague
Computer Vision and System Laboratory (CVSL)
Department of Electrical and Computer Engineering,
Laval University,
Quebec City (Quebec) G1V 0A6, Canada
E-mail: Bardia.Yousefi@ieee.org, clemente.ibarra-castanedo@gel.ulaval.ca, Xavier.Maldague@gel.ulaval.ca

S. Sfarra
University of L'Aquila,
Department of Industrial and Information Engineering and Economics (DIIIE),
Piazzale E. Pontieri no. 1, I-67100, Monteluco di Roio, Roio Poggio - L'Aquila (AQ), Italy
and
Tomsk Polytechnic University, Lenin Av., 30, Tomsk 634050, Russia
E-mail: stefano.sfarra@univaq.it

N. P. Avdelidis
Computer Vision and System Laboratory (CVSL)
Department of Electrical and Computer Engineering,
Laval University,
Quebec City (Quebec) G1V 0A6, Canada
and
Aerospace Integration Research Centre (AIRC)
College Road, Cranfield, MK43 0AL
United Kingdom
E-mail: nico.avdel@gmail.com

(SNMF1) and standard NMF optimized by Non-negative least squares (NNLS) active-set algorithm (SNMF2) and eigen-decomposition approaches such as Principal Component Analysis (PCA) in Thermography, Candid Covariance-Free Incremental Principal Component Analysis (CCIPCA) in Thermography to obtain the thermal features. On one hand, these methods are usually applied as preprocessing before clustering for the purpose of segmentation of possible defects. On the other hand, a wavelet based data fusion combines the data of each method with PCA to increase the accuracy of the algorithm. The quantitative assessment of these approaches indicates considerable segmentation along with the reasonable computational complexity. It shows the promising performance and demonstrated a confirmation for the outlined properties. In particular, a polychromatic wooden statue, a fresco, a painting on canvas, and a building were analyzed using the above mentioned methods and provide up to 71.98%, 57.10%, 49.27%, and 68.53% accuracy of defect (or targeted) region segmentation, respectively.

Keywords Thermal image segmentation · Negative Matrix Factorization Analysis · Gradient-descent-based multiplicative rules · Non-negative least squares (NNLS) active-set algorithm · wavelet data fusion · Clustering.

1 Introduction

Looking into the scientific databases with thermography and cultural heritage as keywords, it is possible to note an increment in the recent years publications (for example [15, 11, 20]). Subsequently, a decrement can be observed. However, the need to pass from a qualitative inspection to a quantitative evaluation grows year by year taking into account the natural disasters which afflict the conservation and safeguarding of cultural heritage. Very recently Davin et al. [4] considered the cooling-down thermography to reveal paintings covered by a limewash layer. The transient infrared image sequence allowed to reconstitute the subsurface pattern by processing the thermal contrast. Yao et al. introduced for the first time the use of the multi-dimensional ensemble empirical mode decomposition technique for the thermographic diagnosis of mosaics [24]. The results obtained after the inspection via a very long pulse were encouraging, above all when compared with the results coming from recent and non-recent algorithms. The infrared thermography (IRT) method was also used in Volterra (Central Italy), that is a town of great historical interest due to its vast and well-preserved cultural heritage. IRT was applied with the aim of detecting possible criticalities on the wall-enclosure, with special regards to moisture and seepage areas. Four thermal anomalies were highlighted [12]. Becherini et al. investigated the causes of the different damage features observed in the stucco statues located into the Longobard Temple in Cividale del Friuli, Udine (Italy). In particular, the surface temperature of the statues was investigated by means of IRT [2]. Contextually, Tang and Dai [21] applied an integrated approach using 3D laser scanning, high-definition digital photography, environmental monitoring, thermal infrared imaging, microwave scanning and penetration resistance tests to study the deterioration of wall paintings conserved in the Chapel of Our Lady of Guia which is a heritage site in the historic

centre of Macau. A robotic system called aIRview was utilized to automatically acquire and process thermal images in a medieval chapel located in N-W of Italy with the aim to evaluate the decay of fresco mural paintings [3]. Signal processing algorithms based on Fast Fourier Transform (FFT) analysis were applied to the acquired data in order to understand the deterioration mechanisms.
In the present paper, the problems caused by the earthquake of 2009, which partially destroyed the city of L'Aquila (Italy) and its surroundings is investigated in three works of art and buildings. The first one is a fresco which was preserved in the Church of Saint Peter Apostle Onna (L'Aquila, Italy) [16,28], the second one is a polychromatic wooden statue representing a Madonna with his Child coming from a village in the province of L'Aquila [17], while the third one is a painting on canvas representing St. Bernardino, i.e., one of the patron of L'Aquila city (Italy). In these cases, the thermographic campaigns were conducted in the Museo di Paludi di Celano (L'Aquila, Italy) where the objects were transported after the quake for a first aid. The thermographic inspections were focused on the detection of sub-superficial cracks, inclusions of heterogeneous materials, splitting areas, and the retrieving of ancient restorations. During the inspections, a restorer indicated the main region of interest (ROI) to be recorded on the basis of personal experience. The radiation source consisted of lamps (no flashes) which provided long thermal stimuli, while in each experimental campaign a ThermaCAM S65 HS by FLIR collected the IRT data. The latter were subsequently analyzed in Matlab environment. In a second thermographic campaign, a building restored after the earthquake of 2009 [6,22] was inspected which involves thermal stimulus coming from the Sun [14] as heating sources.
There are well-known approaches such as Principal Component Thermography (PCA in thermography also called PCT) [13],[35],[34],[36] among many others brunches of PCA with additional penalty terms [5],[30],[32],[29],[31], which have been previously used in the scientific literature for the inspection of artistic objects and buildings. Non-Negative Matrix factorization (NMF) [7] is an approach having a similar decomposition, but non-negative values, if compared to PCA [13]. Two NMF approaches called standard Non-Negative Matrix Factorization (NMF) optimized by gradient-descent-based multiplicative rules (SNMF1) and standard NMF optimized by Non-negative least squares (NNLS) active-set algorithm (SNMF2) are used herein as preprocessing stage [33]. These methods showed considerable performance in terms of magnifying the impaired regions in targets heated by artificial or natural heat sources. This magnification presented a considerable role as a preprocessing step before segmentation. In the same time, they increase the ability of the segmentation on these regions. For segmentation, an unsupervised approach HSV based PCA kernelled clustering was used along with the analysis of computational complexity for each approach [25]. NMF techniques make easier the segmentation process and their results indicate promising performance and demonstrated a confirmation for the outlined properties. These methods provided substantial benefits also in terms of reduction of the computational cost, as well as in the obtaining of clear quantitative results concerning the defects detected. In addition, the emissivity variation effect which is naturally present on polychromatic objects will be greatly reduced. The problem of the emissivity variation [1],[33] is linked to: a) the pigments applied by the art masters on the upper layers, and b) the thermal stimuli induced by lamps

which is useful to generate a 3D thermal transient. Statistical approaches are generically applied on raw thermograms, the aforementioned adverse effect is significantly reduced and seems ineffectual for segmentation. In the next section, the materials and methodology of the approach will be briefly described with different thermal image decomposition analysis that are used along with the segmentation process. The experimental and computational results, as well as the discussion are then presented in Sections 4, 5, respectively. The conclusions Section is finally illustrated in Section 6.

2 Main information concerning the inspected objects

2.1 Wooden statue

Taking into account the defects' shape (i.e., round defects), as well as the restoration phase recently performed on the statue (which removed the defects themselves), it is possible to say that they correspond to inclusions of foreign materials. One of these defects, visible near to the left ear of the Child and indicated in Figure 1.a may be linked to the remodeling of the Child's face over time. The dimensions of the defects on the plane were approximately identical. The Figure provides an idea about the defect dimension which can be roughly assimilate to a coin of 1 euro. The two defects (the second one not detectable to the naked eye, but magnificently visible after the application of the advanced image processing techniques) were present beneath the plaster layers. In fact, plaster undergone different final treatments in order to guarantee the best conditions to the paint layer. Nevertheless, the craquelure effect appeared over time on the face of the Child, although only the inserts were analyzed/segmented.

2.2 Fresco

The fresco painting used in this case is a method of painting water-based pigments on freshly applied plaster on wall surfaces. The colours were made by grinding dry-powder pigments in water, dry and set with the plaster became a permanent part of the wall. The correctly prepared intonaco holded its moisture for many hours. When the painter diluted his colours with water and applied them with bruchstrokes to the plaster, the colours were imbibed into the surface, and as the wall dried and set, the pigment particles became bound or cemented along with the lime and sand particles. This gave to the colours great permanence and resistance to aging, since they are an integral part of the wall surface, rather than a superimposed layer of paint on it. The fresco has undergone a rotation process; it was recovered by the firefighters with the painted surface faced the floor (Figure 1.b). Because of this, cracks appeared on the surface also afflicting the inner layers. The restoration phase of the fresco started into the Museo delle Paludi di Celano (L'Aquila Italy) where the restorers applied protective films in order to stop the propagation of the cracks. Interestingly, the cracks can be visualized by applying the infrared thermography method above the protective films. In particular, three cracks started from the The circle is missing in the Figure. Please check and/or modify Figure 1.b.

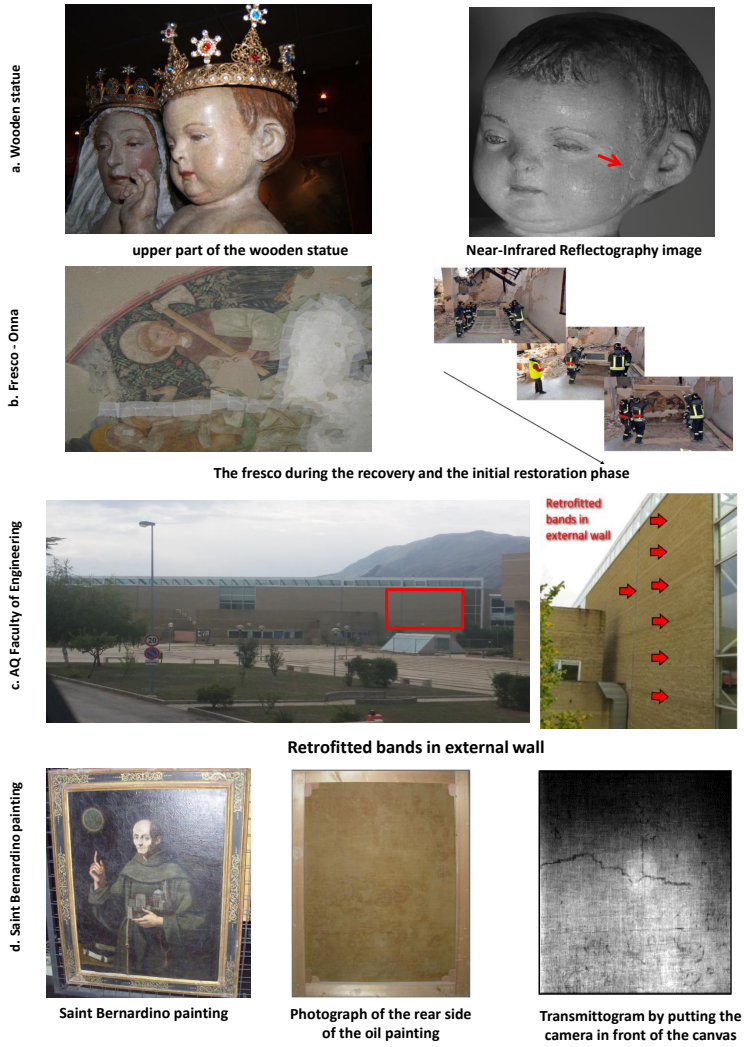

Fig. 1 The specimens used for infrared inspection are shown. (a) shows the wooden statue with the location of one defect. (b) presents a part of the inspected fresco along with recovery of the fresco by the firefighters. (c) Retrofitted bands in external wall. (d) Saint Bernardino painting, photograph of the front and rear side of the oil painting, A transmittogram is also shown by putting the camera in front of the canvas and the illuminating source in front of the varnish layer.

2.3 The facade of the Faculty of Engineering of L'Aquila

The new building of the Faculty of Engineering of L'Aquila University was partially destroyed during the 2009 earthquake. The reconstruction of the building was accomplished in 2013, although the latest final additions were performed in 2016. During this process, several internal and external walls were retrofitted using a flax fiber re-

inforced polymer (FFRP) (FIDFLAX UNIDIR 430 HS43) that was applied in recursive lines (vertical and horizontal). They are also called retrofitted bands in the wall (Figure1.c). In the region of interest (ROI) analyzed, three horizontal and one vertical lines were recorded. The fibers were glued to the support by using a thermoplastic matrix (i.e., an epoxy resin). In the other parts of the facade, parallelepiped bricks resembling tufaceous material were used. The idea was to detect the four recursive lines present into the ROI analyzed.

2.4 St. Bernardino painting

The oil painting on canvas (1500 $\times$ 1100 mm) was painted by Giulio Cesare Bedeschini from 1610 to 1613. In this painting, San Bernardino appears holding the City of L'Aquila in his left hand. The Basilica of San Bernardino can be seen in the condition in which it was at the beginning of 17^{th} century. The oil painting is a multilayer structure composed by (from bottom to top), a canvas in linen, a glue size layer, a ground layer, oil paint layers of different thicknesses, and a varnish. A large crack can be identified, going from the right shoulder of the character towards the bust. The crack can even be detected through the wood frame on the right side. On the left side, going to the top of San Bernardino's right hand, there is a slight indication of a possible continuation of the crack (Figure 1.d). Detachments in the wooden frame were identified as well. The crack is not visible from the rear side (Figure 1.d), but the transmittogram in the same figure (left image at Figure 1.d) detected it with a good contrast. A complementary metal-oxide semiconductor camera was used during the near-infrared acquisitions. This is a clue that the linen canvas can be double possibly chosen at that time by artmasters.

3 Methodology

The methodology is summarized by presenting an algorithm for defect segmentation in Non-destructive Testing (NDT) that involves several thermal image decomposition analysis, data fusion, and clustering. Here, a brief summary of the image decomposition algorithms is presented as dimension reduction approaches (Figure 2 and Algorithm 1), which considers a preprocessing step before segmentation through K-means clustering.

3.1 A brief review on Eigen decomposition thermography

PCA in thermography [13] is considered as one of the very efficient decomposition methods in finding defects, as well as reducing thermographic data. Singular Value Decomposition (SVD) as a statistical method is used to improve the performance of PCA. In general, matrix X is $n \times p$ and can be decomposed as follows:

$$X = U\Gamma V^T \tag{1}$$

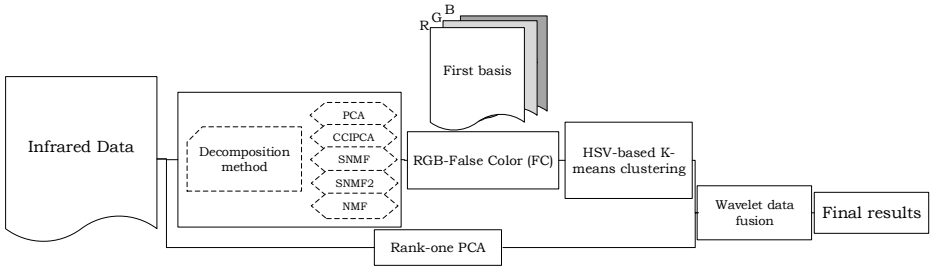

Fig. 2 The scheme of our proposed algorithm is presented.

Let $p > n$ and considering Γ to be a diagonal matrix $n \times n$ having zero or positive elements showing the singular values of matrix X, where U is $p \times n$ matrix, and V^T is the transpose of $n \times n$ matrix. The data is arranged based on the time variations column-wise along with the spatial changes which occur row-wise and can be presented in the columns of matrix U [13] (each frame is vectorized and concatenates to other). Candid Covariance-Free Incremental Principal Component Analysis (CCIPCA) in Thermography (CCIPCT) [27],[26] is an algorithm that iteratively computes the eigenvalues and eigenvectors. This provides lower computational complexity as compare to PCA for high dimensional data also gives low-rank outcome and possibility to calculation the process in the online paradigm.

3.2 Non-negative matrix factorization

The non-negative matrix factorization (NMF) in the standard form involves decomposing a non-negative matrix $X \in R^{m \times n}$ to two non-negative factors $Y \in R^{k \times n}$ and $A \in R^{m \times k}$ (for $k < min(m,n)$), that is

$$X_+ = A_+ Y_+ + E, \tag{2}$$

$$min \quad \frac{1}{2} \parallel X - AY \parallel_F^2 \quad subject\ to, A, Y \geq 0 \tag{3}$$

This formula was derived from log-likelihood function under a Gaussian error assumption. The matrix A is called the basis matrix from the thermographic image, Y is the coefficient matrix, and the Xs columns are the multivariate data points. The data point is a linear combination of the basis vectors that are (sparse) non-negative and non-convex optimization problem. One of the solution for such a problem is block-coordinate descent [7]. The optimization uses non-negative least squares (NNLS) considering A and Y. Here, the input thermography data is the basis calculated by NMF optimised by two different GD and NNLS methods [18].

Algorithm I

Given Input data **I(x,y,z)** $\in \boldsymbol{R^{N\times M\times Z}}$ which **I(x,y)** $\in \boldsymbol{R^{N\times M}}$ is spatial dimension for infrared image selected and its unit is pixels, **z** represents the frequency of acquisition.

Step 1 Calculation of factor analysis

$$\mathbf{M}_{\boldsymbol{k}}\,(\boldsymbol{x},\boldsymbol{y}) = \boldsymbol{FA_j}\,(\boldsymbol{I}(\boldsymbol{x},\boldsymbol{y},\boldsymbol{z}))$$

$\boldsymbol{k}$ is number of the eigen-images taken selected for the analysis. $\boldsymbol{FA}$ presents the technique uses for decomposing the input data and $\boldsymbol{j}$ shows the types of techniques(*e.g.* j=1 corresponds to PCA). $\boldsymbol{M_k}(\boldsymbol{x},\boldsymbol{y})$ shows the $\boldsymbol{k}$ eigen-image of input data, $\boldsymbol{k} < \boldsymbol{z}$.

Step 2 Manually selecting $\boldsymbol{M}_i(\boldsymbol{x},\boldsymbol{y})$, $\boldsymbol{i^{th}}$ eigen-image

$$\grave{\mathbf{M}}_i(\boldsymbol{x},\boldsymbol{y},\mathbf{3}) \overset{FC}{\rightarrow} \boldsymbol{M}_i(\boldsymbol{x},\boldsymbol{y})$$

Where $\grave{\mathbf{M}}_i(\boldsymbol{x},\boldsymbol{y},\mathbf{3})$ shows the false color (FC) RGB matrix of $\boldsymbol{M}_i(\boldsymbol{x},\boldsymbol{y})$.

Step 3 Clustering calculation for segmentation purpose.

$$\grave{\mathbf{M}}_{\mathbf{i}}(\boldsymbol{x},\boldsymbol{y},\mathbf{3}) \overset{\boldsymbol{HSV}}{\longrightarrow} \boldsymbol{X}(\boldsymbol{a_i})_{\boldsymbol{i}=\mathbf{1,2,3}}$$

$$\boldsymbol{A}(\boldsymbol{x},\boldsymbol{y},\boldsymbol{K}) = \boldsymbol{min}_{\boldsymbol{C},\boldsymbol{a_j}} \sum_{\boldsymbol{c}=\mathbf{1}}^{\boldsymbol{K}} \sum_{\boldsymbol{j}=\mathbf{1}}^{\mathbf{3}} \|\boldsymbol{X}(\boldsymbol{a_i}) - \boldsymbol{m_c}\|^{\mathbf{2}}$$

$X(a_i)$ is shown the HSV color system matrix of $\grave{\mathbf{M}}_{\boldsymbol{k}}(\boldsymbol{x},\boldsymbol{y},\mathbf{3})$. Let $\boldsymbol{m_c}$ be the average value of data. $\mathbf{K}$ is shown the initial number of the clusters. Where the $\boldsymbol{A}(\boldsymbol{x},\boldsymbol{y},\boldsymbol{K})$ represents the segmented region.

Step 4 Calculating the second part of analysis using PCA:

$$\boldsymbol{\Phi}_{\boldsymbol{\gamma}}(\boldsymbol{x},\boldsymbol{y}) = \boldsymbol{FA_1}\,(\boldsymbol{I}(\boldsymbol{x},\boldsymbol{y},\boldsymbol{z}))$$

$\boldsymbol{\Phi}_{\boldsymbol{\gamma}}(\mathbf{x},\mathbf{y})$ shows the $\boldsymbol{\gamma^{th}}$ manually selected eigen-image. Applying thresholding (δ), $\boldsymbol{\Phi}_{\boldsymbol{\gamma}}^{\boldsymbol{\delta}}(\boldsymbol{x},\boldsymbol{y})$. δ obtained from $\boldsymbol{I}(\boldsymbol{x},\boldsymbol{y},\boldsymbol{z}')$ ($\boldsymbol{z}' \in \boldsymbol{R^{Z'}}$, $\boldsymbol{z} \in \boldsymbol{R^{Z}}, \boldsymbol{Z}'\Delta\,\boldsymbol{Z}$).

Output Calculating Wavelet data fusion

$$\boldsymbol{C}(\boldsymbol{x},\boldsymbol{y}) = \boldsymbol{\omega^{-1}}\left[\boldsymbol{\phi}\left(\boldsymbol{\omega}[\boldsymbol{A}(\boldsymbol{x},\boldsymbol{y},\dot{\boldsymbol{K}})], \boldsymbol{\omega}\left[\boldsymbol{\Phi}_{\boldsymbol{\gamma}}^{\boldsymbol{\delta}}(\boldsymbol{x},\boldsymbol{y})\right]\right)\right]$$

Where $\boldsymbol{A}\left(\boldsymbol{x},\boldsymbol{y},\dot{\boldsymbol{K}}\right)$ is the best representative of defect through different $\dot{\boldsymbol{K}} \leq \boldsymbol{K}$.

3.3 The 2-D wavelet transform implementation for multiresolution decomposition images

Applying the aforementioned techniques as preprocessing techniques requires further process due to complementary properties of the applied methods that help to add and eliminate the good and bad performance, respectively. For that, data fusion is a solution and leads to the pyramid-structured wavelet decomposition [10] and following [19], the multiresolution wavelet decomposition(1D) extended to 2D by separately introducing of every dimension (in 2D) to wavelet functions and scaling as the tensor products of 1D. The 2D wavelet analysis operation consists of sets of filtering and down sampling in horizontal and vertical directions. Wavelet data fusion considers one of data transformation similar to wavelet transform itself [8], [14]. The methodology for data fusion applying wavelet includes transforming data to wavelet domain, fuse them and transform the results back to the spatial domain. Here, one side of this fusion is always the manually best representative score of PCA and other side changes in different methods. The reconstructed data fusion used in the proposed approach is shown by:

$$C(\varepsilon) = \omega^{-1}[\phi(\omega[A(\varepsilon)], \omega[V^{i}_{PCA}(\varepsilon)])] \tag{4}$$

Where the wavelet transformation is presented ω and let (ε) is eigen image obtained by one of the input data decomposition approaches (eigen-images applying one of the approaches) and $V^{i}_{PCA}(\varepsilon)$ is a manually selected eigen-image obtained by PCA. It is noticeable that this eigen-image needs to be manually selected and being used in the system. This data fusion takes place through ϕ fusion rules. $C(\varepsilon)$ represents the fused data through the inverse wavelet transform represented by ω^{-1}.

3.4 K-means clustering

There are countless research works that involve K-means algorithm for data clustering, e.g. [9]. Here, a brief review of the K-means is presented.
Suppose $S = X_1, \ldots, X_n \subseteq R^p$ is our observation set and dissimilarities are $\|X_i - X_j\|_2^2$ for $X_i \in R^p$ and K is the number of clusters. Clustering of the data X is nothing more than a function C assigning every observation X_i to a set of $k \in 1, \ldots, K$. The minimization of the following formula is required:

$$J_k = \sum_{k=1}^{K} \sum_{C(i)=k} \|X_i - \bar{X}_k\|_2^2 \tag{5}$$

Let $X = 1/n \sum_{i=1}^{n} X_i$ and $C(i) = k$ means that X_i is assigned to group k.

4 Experimental Results

The experimental setup of the polychromatic statue, the fresco, the building restored and the painting on canvas, are shown in Figures 3 a-d, respectively. The authors also

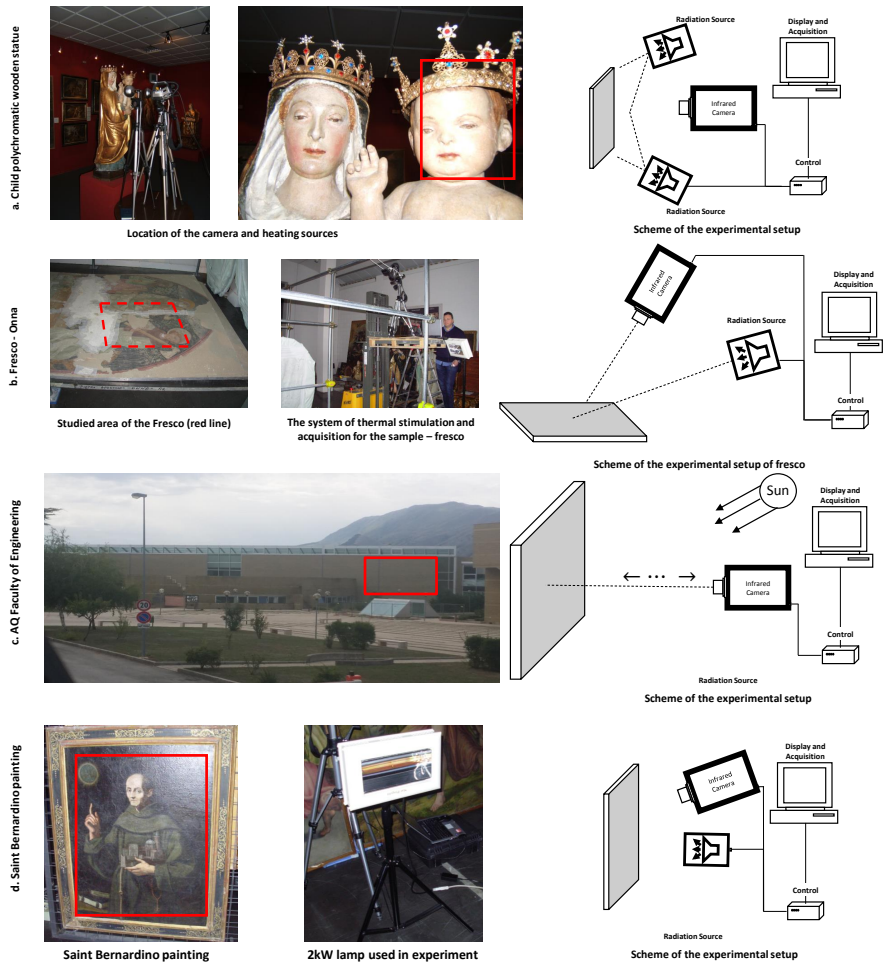

Fig. 3 Experimental setups and conditions of acquisition for each thermographic test. a) Child polychromatic wooden statue; b) fresco; c) AQ Faculty of Engineering; d) Saint Bernardino painting.

compared the computational results for different factor analysis and eigen decomposition techniques in the algorithm to analyze the performance of them by segmenting the defects.

4.1 Experimental set up

Concerning the statue, the test conducted to gather the infrared images in the laboratory environment and the experimental set up are shown in Figure 3.a. The successful thermography test partially depends on the camera operation spectrum and the source

of infrared. The infrared camera used was a long wave infrared camera (LWIR, 7.5 - 13 μm) having the spatial resolution of 240×320 pixels. There were two radiation sources, i.e., two 250 W SICCATHERM E27 lamps that gave a wide radiation spectrum for thermography testing. As the overheating is always a concern in the cultural heritage field, the temperature of the target was monitored during the test using a laser pyrometer. The ambient temperature was approximately 292K $(19^{\circ}C)$ at the starting of the thermographic inspection. During the test, the infrared thermography acquisition process was also controlled using the spot function, while the lamps were located far from the specimens $(24cm)$ to provide an adequate heating up phase. The distance between the lamps was $40cm$, while the thermal camera was placed $40cm$ from the left cheek of the Child wooden statue. The relative humidity (RH) was 47.5% and the emissivity value was established at 0.90. The six hundred thermograms were recorded during 180 seconds of heating and seven minutes of cooling (420 thermograms).
In the experiment of the real fresco, the heating up phase lasted 360 seconds. The camera was located at $295cm$ from the sample surface, while 1 lamp (2kW) was put at the distance of $235cm$. The ambient temperature recorded was 16.2 $^{\circ}C$, while the RH was equal to 40.1%. Taking into account the high roughness of the surface, the emissivity value was set at 0.90, although the techniques explained in section 2 tend to minimize the emissivity variation due to the pigments. The cooling down phase lasted 780 seconds, and 1 thermogram per second was recorded during the entire inspection procedure. The experimental setup is shown in Figure 3.b.
In contrast to other experiments, the experiment inherent to the Faculty of Engineering of L'Aquila city was performed in passive thermographical conditions. During the image acquisition, the infrared camera was located very far with respect to the targeted wall which is shown in Figure 3.c.
In the case of St. Bernardino, the painting was heated with a 2 kW lamp installed in front of the paint surface at 230 cm. Instead, the distance between the camera and the sample (working in reflection mode) was 280 cm. The ambient temperature was 16.2 $^{\circ}C$, the relative humidity of 40.2 % and emissivity value established in 0.80. The thermograms recorded were 600 in total; in particular, 180 seconds of heating and 420 seconds of cooling were a prior selected (Figure 3.d).
Both the computation and the algorithm were run in a PC (Intel (R) Core(TM) i7 CPU, 930, 2.2.80GHz, RAM 12.00GB, 64 bit Operating System) and the processing was conducted using MATLAB computer program. The results of eigen-decomposition analysis techniques and the simulation results of each step of the proposed algorithm is shown in Figure 4 and Tables 1-3. Each of the decomposition methods have some pros and cons that provide certain strengths or weaknesses to extract the defects in the test. Here, the sensitivity of these methods is investigated to increase the performance of the algorithm in order to segment the defects. Figure 5.a shows the results of the eigen-decomposition techniques of the child. The results of the methods for fresco is presented in Figure 3.b. All the methods revealed considerable outcome to extract the defects on a part of the polychromatic wooden statue minus SNMF1, which was able to detect only the deeper defect. The results of fresco revealed also a considerable performance of CCIPCA, NMF, PCA, SNMF1. However, the SNMF2 provided more misclassified regions (which is qualitatively shown in Figure 4.b) than others. Intriguing, sub-superficial cracks can be easily detected as indicated by red arrows.

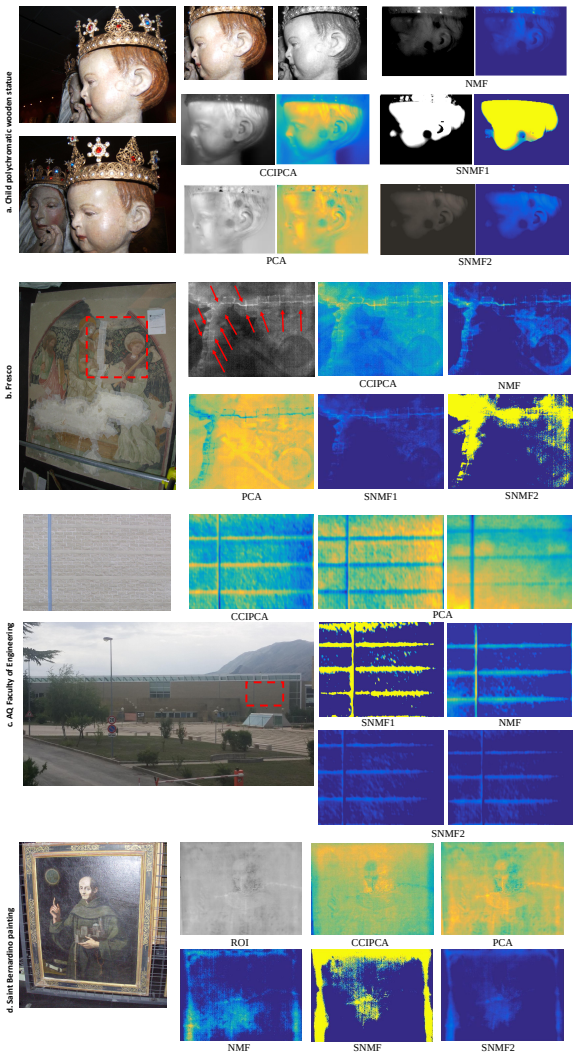

Fig. 4 Results of eigen decomposition techniques. a) Child polychromatic wooden statue; b) fresco; c) AQ Faculty of Engineering; d) Saint Bernardino painting. In every case the results of CCIPCA, PCA, NMF, SNMF and SNMF2 are presented.

Contrarily, in CCIPCA and PCA the false positive has lower amount as compare to others, which is confirmed by quantitative results in table 2. For one detected defect (it is shown in Figure 4.a, i.e., the lower defect on the face of child statue) SNMF1 has high accuracy if compared to the other methods (Table 1). CCIPCA has also manifested the highest accuracy considering lower false positive (100% accuracy - 0.69% false positive). However, the accuracy of the proposed approach considerably decreased when the second defect is also added to the calculations (the second defect

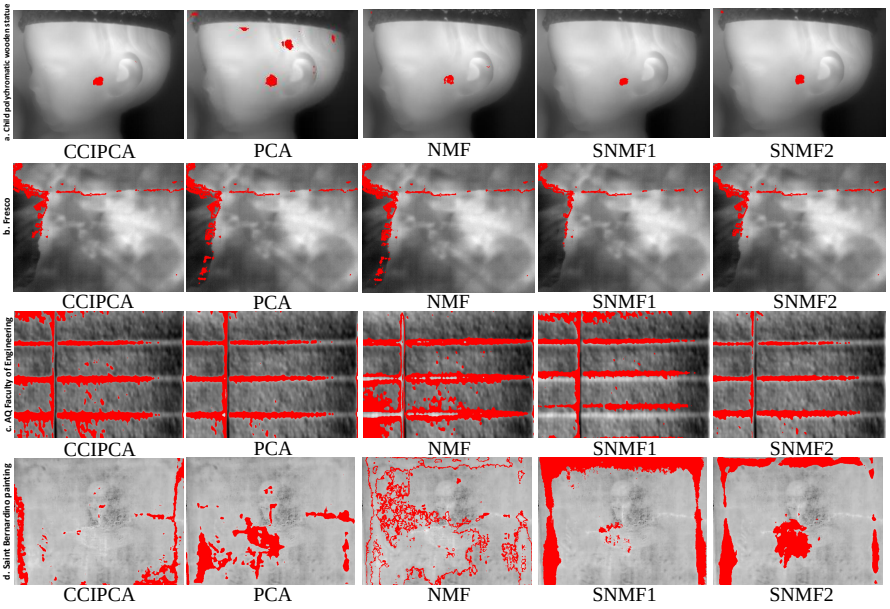

Fig. 5 The final results of the proposed algorithm for defect detection and automatic detection/classification of externally reinforced structures composed by flax fiber reinforced polymer (FFRP) composites.

located on the surface of the Child). See for reference Figure 3a, i.e., the higher defect on the face of child statue which is smaller than the first detected and Table 2). The wavelet data fusion provided a good data combination to decrease the effects of misclassification and increase the influence of good segmentation. For instance, on one hand PCA provides performance, which can be added to the rest of the methods and on the other hand, the additional methods give some misclassified regions in terms of false positives (extra detected defects) that can be eliminated through this data fusion. The results of the all techniques are shown in the Figure 5. The computational load [1] of the methods are comparatively shown in tables 3. It is noticeable that CCIPCA has the lowest computational complexity, therefore it is a fast and accurate technique to be used into the cultural heritage field, as well as for the automatic detection/classification of externally reinforced structures composed by flax fiber reinforced polymer (FFRP) composites in buildings. It is possible to mention that the difference in the accuracy is also linked to the way in which the different algorithms ”react” to the emissivity variation caused by the pigments or natural fibers.

[1] The computational load is processing time measured while the computer system performs (CPU time).

Table 1. The quantitative accuracy of our approach for the polychromatic statue is shown; in this case the authors consider only one defect detected on the specimen surface.

Methods	Accuracy			
	Pixels detected correctly (True positive)	**Accuracy (%)**	**False-positive**	**False-positive (%)**
PCA	1292	100	387	29.95
NMF	386	98.13	39	10.45
CCIPCA	1445	100	10	0.69
SNMF	551	99.81	0	0
SNMF2	983	100	70	7.12

Table 2. The quantitative accuracy of our approach for the polychromatic statue, the fresco, the Faculty of Engineering of L'Aquila city, and the painting on canvas is shown.

Methods	**Accuracy** (polychromatic statue)					
	Pixels detected correctly (True positive)	**Accuracy (%)**	**False Negative**	**False Negative (%)**	**False Positive**	**False Positive (%)**
PCA	2178	42.35	1841	35.79	17	0.33
NMF	3627	70.52	423	8.23	12	0.23
CCIPCA	1899	36.92	3244	63.08	1536	29.87
SNMF	1355	26.35	3538	68.79	42	0.81
SNMF2	3702	71.98	718	13.96	1050	20.41
Methods	**Accuracy** (fresco)					
	Pixels detected correctly (True positive)	**Accuracy (%)**	**False Negative**	**False Negative (%)**	**False-positive**	**False-positive (%)**
PCA	3140	57.11	2359	42.89	3187	57.96
NMF	3007	54.68	2492	45.32	2217	40.32
CCIPCA	2890	52.55	2609	47.45	1770	32.18
SNMF	3007	54.68	2492	45.32	2217	40.32
SNMF2	2919	53.08	2580	46.92	1318	23.97
Methods	**Accuracy** (Faculty of Engineering AQ's wall)					
	Pixels detected correctly (True positive)	**Accuracy (%)**	**False Negative**	**False Negative (%)**	**False-positive**	**False-positive (%)**
PCA	19850	68.53	9115	31.47	13136	45.35
NMF	16341	56.42	12624	43.58	12233	42.23
CCIPCA	19677	67.93	9288	32.07	13082	45.16
SNMF	16013	55.14	13027	44.86	3477	11.97
SNMF2	14886	51.26	3082	48.74	3082	10.61
Methods	**Accuracy** (St. Bernardino painting)					
	Pixels detected correctly (True positive)	**Accuracy (%)**	**False Negative**	**False Negative(%)**	**False-positive**	**False-positive (%)**
PCT	3071	30.49	7190	3.83	16515	8.78
NMF	4223	41.94	6013	3.19	61149	32.53
CCIPCT	4961	49.27	5770	3.07	10786	5.74
SNMF	3430	34.06	7190	3.83	33108	17.61
SNMF2	2649	26.31	7641	4.06	26167	13.92

4.2 Results of the clustering

The results of eigen decomposition and factor analysis techniques have been presented in the previous section, while in this section the results for K-means clustering are shown in Figure 5. They include the clustering approach for the algorithm in every

Table 3. Table of computational cost for the proposed methods inherent to the polychromatic statue, fresco, Faculty of Engineering AQ's wall, and the painting on canvas.

Methods	**Computational load** (polychromatic statue)		
	Factor analysis (s)	**Clustering (s)**	**Wavelet fusion (s)**
PCA	1.570819	0.92	0.022
NMF	4.267770	0.72	0.02
CCIPCA	0.024910	1.19	0.021
SNMF	(for 1000 Iteration) 30.994544	0.84	0.018
SNMF2	(for 200 Iteration) 53.151630	0.722	0.032
Methods	**Computational load** (fresco)		
	Factor analysis (s)	**Clustering (s)**	**Wavelet fusion (s)**
PCA	9.678299	0.484188	0.011242
NMF	7.290876	2.285472	0.013743
CCIPCA	0.204019	0.112533	0.007896
SNMF	(for 1000 Iteration) 119.111053	0.169409	0.007228
SNMF2	(for 200 Iteration) 227.278529	0.092327	0.094902
Methods	**Computational load** (Faculty of Engineering AQ's wall)		
	Factor analysis (s)	**Clustering (s)**	**Wavelet fusion (s)**
PCA	7.862273	0.430725	0.008992
NMF	6.508169	0.846036	0.009688
CCIPCA	0.075162	0.330999	0.008949
SNMF	(for 1000 Iteration) 115.798613	0.589722	0.010877
SNMF2	(for 200 Iteration) 206.573677	0.558081	0.047884
Methods	**Computational load** (St. Bernardino painting)		
	Factor analysis (s)	**Clustering (s)**	**Wavelet fusion (s)**
PCA	4.390504	1.438757	0.389003
NMF	6.980534	0.460320	0.034915
CCIPCA	2.282091	0.736115	0.040203
SNMF	(for 1000 Iteration) 76.142209	0.961962	0.069831
SNMF2	(for 200 Iteration) 129.605149	0.86453	0.05457

dimensional reduction techniques. As it aforementioned, the applying of clustering in different methods and fuse the data with PCA creates best possible similar outcome. Figure 5 qualitatively shows the performance of the clustering approach after wavelet data fusion for different procedures. Tables 1,2 represent the accuracy and computational load of the algorithm to find defects or automatically classify natural fibers applied on the facade of a building, respectively. To quantitatively evaluate the accuracy of the proposed algorithm, a ground truth (GT) is required. For that, an image that is manually labeled has been used. Besides the accuracy of defect detection which considers a significant difference between these methods, computational load of the approach and clustering are some other differentiation factors in our analyzes. Local accuracy (ACC) is calculated by:

$$ACC(\%) = \frac{Correct\ detected\ pixels}{Total\ pixels\ of\ defect} * 100 \tag{6}$$

The accuracy was calculated based on the number of detected pixels and were compared to GT images (false-positive and false-negative parts were also eliminated from the raw accuracy). A professional art and archeology restorer - having several years of

experience - worked on the validation of the defects detected, subsequently repaired in part or totally. This technical help increased the reliability of the procedure.

5 Discussion

Application of the thermal image analysis using PCA, CCIPCA, SNMF1, and SNMF2 were proposed for defect detection. The main concerns for automated system to find the defects using mentioned approaches is to find best basis image which better represents the ROI (the basis corresponds to which rank). Choosing lower number of basis, normally provides no guarantee to have better defect representation. CCIPCA improves the problem of batch analysis of PCA and strives to alleviate the rank selection problem [23],[26] but yet provides lower contrast property than PCA. It is the reason for which the second defect in Child polychromatic wooden statue is solely detected in PCA (it is also shown in CCICPA, NMF, and SNMF2 but did not automatically detected, Figure 4) and better visibility of defect in the mural painting through PCA (Figure 5). However, Saint Bernardino painting result for CCIPCA is better than PCA and apparently all of the methods because of low rank performance of CCIPCA (lesser mixing up the basis) but still showed lower contrast as compared with other methods. Since NMF basically has non-negative coefficients correspond to basis, unlike PCA and CCIPCA, the selected basis can be more representative of different classes in segmentation performance but yet they showed relatively similar performance. The optimization of NMF by gradient descent, which ensures the convergence by rescaling factor in thermography application, did not show any significant difference as compared to the conventional least squares error minimization nor the generalized Kullback-Leibler divergence. One very good example of this point is shown in the results of SNMF1 and SNMF2 in Child polychromatic wooden statue (Figure 5).

6 Conclusions

The proposed approach was based on applications of thermal and infrared technology in Civil engineering, Arts and Archeology fields. It addressed the application of some known factor analysis and eigen-decomposition methods such as standard Non-Negative Matrix Factorization (NMF) optimized by gradient-descent-based multiplicative rules (SNMF1) and standard NMF optimized by Non-Negative Least Squares (NNLS) active-set algorithm (SNMF2) and Principal Component Analysis (PCA in Thermography), Candid Covariance-Free Incremental Principal Component Analysis(CCIPCA) in Thermography to obtain the thermal features. These methods have been applied as preprocessing before clustering for segmentation purpose of possible defects (and/or retrieval/detection of natural fibers used to rebuild buildings). In addition, a wavelet based data fusion was used to combine the data of each method with PCA. In this way, the accuracy of the algorithm was increased. Three different artistic specimens, a polychromatic statue, a fresco, and a painting on canvas, have been used to benchmark the proposed algorithm, along with an external wall reinforced by natural fibres. The quantitative assessment of these approaches indicates

considerable segmentation along with the reasonable computational complexity. It showed the promising performance for most of the decomposition method particularly for CCIPCA (low computational load and reasonable accuracy) and demonstrated a confirmation for the outlined properties. Both from a mathematical and engineering point of view, interesting results were obtained. The future work will include the analysis of the algorithm for other data-set to evaluate its strength and weakness.

Acknowledgement

The authors would thank anonymous reviewers and Journal of Thermal Analysis and Calorimetry's editor for their constructive comments. We would like to thank Geltrude Di Matteo (director) and Alessandro Verrocchia (chief restorer), of the Musè (Il Museo delle Paludi di Celano) Italy, for their kind cooperation in this work. The authors also want to acknowledge the support of the Multipolar Infrared Vision Canada Research Chair (MIVIM), tier 1. A special thank to Mr. Giovanni Pasqualoni of the University of L'Aquila (L'Aquila, Italy), for the technical support during the thermographic acquisitions.

References

1. Avdelidis, N., Moropoulou, A.: Emissivity considerations in building thermography. Energy and Buildings **35**(7), 663–667 (2003)
2. Becherini, F., Bernardi, A., Di Tuccio, M.C., Vivarelli, A., Pockelè, L., De Grandi, S., Fortuna, S., Quendolo, A.: Microclimatic monitoring for the investigation of the different state of conservation of the stucco statues of the longobard temple in cividale del friuli (udine, italy). Journal of Cultural Heritage **18**, 375–379 (2016)
3. Cadelano, G., Bison, P., Bortolin, A., Ferrarini, G., Peron, F., Girotto, M., Volinia, M.: Monitoring of historical frescoes by timed infrared imaging analysis. Opto-Electronics Review **23**(1), 102–108 (2015)
4. Davin, T., Serio, B., Guida, G., Pina, V.: Spatial resolution optimization of a cooling-down thermal imaging method to reveal hidden academic frescoes. International Journal of Thermal Sciences **112**, 188–198 (2017)
5. Ibarra-Castanedo, C., Piau, J.M., Guilbert, S., Avdelidis, N.P., Genest, M., Bendada, A., Maldague, X.P.: Comparative study of active thermography techniques for the nondestructive evaluation of honeycomb structures. Research in Nondestructive Evaluation **20**(1), 1–31 (2009)
6. Ibarra-Castanedo, C., Sfarra, S., Paoletti, D., Bendada, A., Maldague, X.P.: Nondestructive testing of externally reinforced structures for seismic retrofitting using flax fiber reinforced polymer (ffrp) composites. In: Proc. of SPIE Vol, vol. 8705, pp. 87,050U–1 (2013)
7. Lee, D.D., Seung, H.S.: Algorithms for non-negative matrix factorization. In: Advances in neural information processing systems, pp. 556–562 (2001)
8. Li, H., Manjunath, B., Mitra, S.K.: Multi-sensor image fusion using the wavelet transform. In: Image Processing, 1994. Proceedings. ICIP-94., IEEE International Conference, vol. 1, pp. 51–55. IEEE (1994)
9. MacQueen, J., et al.: Some methods for classification and analysis of multivariate observations. In: Proceedings of the fifth Berkeley symposium on mathematical statistics and probability, vol. 1, pp. 281–297. Oakland, CA, USA. (1967)
10. Mallat, S.G.: A theory for multiresolution signal decomposition: the wavelet representation. IEEE transactions on pattern analysis and machine intelligence **11**(7), 674–693 (1989)

11. Mercuri, F., Zammit, U., Orazi, N., Paoloni, S., Marinelli, M., Scudieri, F.: Active infrared thermography applied to the investigation of art and historic artefacts. Journal of thermal analysis and calorimetry **104**(2), 475 (2011)
12. Nolesini, T., Frodella, W., Bianchini, S., Casagli, N.: Detecting slope and urban potential unstable areas by means of multi-platform remote sensing techniques: The volterra (italy) case study. Remote Sensing **8**(9), 746 (2016)
13. Rajic, N.: Principal component thermography for flaw contrast enhancement and flaw depth characterisation in composite structures. Composite Structures **58**(4), 521–528 (2002)
14. Rockinger, O.: Image sequence fusion using a shift-invariant wavelet transform. In: Image Processing, 1997. Proceedings., International Conference on, vol. 3, pp. 288–291. IEEE (1997)
15. Scudieri, F., Mercuri, F., Volterri, R.: Non-invasive analysis of artistic heritage and archaeological findings by time resolved ir thermography. Journal of thermal analysis and calorimetry **66**(1), 307–314 (2001)
16. Sfarra, S., Ibarra-Castanedo, C., Paoletti, D., Maldague, X.: Infrared vision inspection of cultural heritage objects from the city of l'aquila, italy and its surroundings. Materials Evaluation **71**(5), 561 – 570 (2013)
17. Sfarra, S., Ibarra-Castanedo, C., Ridolfi, S., Cerichelli, G., Ambrosini, D., Paoletti, D., Maldague, X.: Holographic interferometry (hi), infrared vision and x-ray fluorescence (xrf) spectroscopy for the assessment of painted wooden statues: a new integrated approach. Applied Physics A: Materials Science & Processing **115**(3), 1041 – 1056 (2014)
18. Sfarra, S., Marcucci, E., Ambrosini, D., Paoletti, D.: Infrared exploration of the architectural heritage: from passive infrared thermography to hybrid infrared thermography (hirt) approach. Materiales de Construcción **66**(323), 094 (2016)
19. Stollnitz, E.J., DeRose, A.D., Salesin, D.H.: Wavelets for computer graphics: a primer. 1. IEEE Computer Graphics and Applications **15**(3), 76–84 (1995)
20. Šulcová, P., Šesták, J., Menyhárd, A., Liptay, G.: Some historical aspects of thermal analysis on the mid-european territory. Journal of Thermal Analysis and Calorimetry **120**(1), 239–254 (2015)
21. Tang, Z., Dai, S.B.: Installation of an environmental monitoring system in the chapel of our lady of guia, macau. Studies in Conservation **61**(sup1), 37–45 (2016)
22. Thakur, V.K., Thakur, M.K., Kessler, M.R.: Handbook of Composites from Renewable Materials, Biodegradable Materials, vol. 5. John Wiley & Sons (2017)
23. Tillmann, A.M., Pfetsch, M.E.: The computational complexity of the restricted isometry property, the nullspace property, and related concepts in compressed sensing. IEEE Transactions on Information Theory **60**(2), 1248–1259 (2014)
24. Yao, Y., Sfarra, S., Ibarra-Castanedo, C., You, R., Maldague, X.P.: The multi-dimensional ensemble empirical mode decomposition (meemd). Journal of Thermal Analysis and Calorimetry pp. 128 (2017) 1841 – 1858.
25. Yousefi, B., Fleuret, J., Zhang, H., Maldague, X.P., Watt, R., Klein, M.: Automated assessment and tracking of human body thermal variations using unsupervised clustering. Applied Optics **55**(34), D162–D172 (2016)
26. Yousefi, B., Sfarra, S., Ibarra-Castanedo, C., Maldague, X.P.: Comparative analysis on thermal nondestructive testing imagery applying candid covariance-free incremental principal component thermography (ccipct). Infrared Physics and Technology **INFPHY-2017-146** (2017)
27. Yousefi, B., Sfarra, S., Ibarra-Castanedo, C., Maldague, X.P.: Thermal ndt applying candid covariance-free incremental principal component thermography (ccipct). In: Thermosense 2017, pp. 10,214–58. SPIE (2017)
28. Yousefi, B., Sfarra, S., Maldague, X.P.: Quantitative assessment in thermal image segmentation for artistic objects. In: Optics for Arts, Architecture and Archaeology, pp. 10,331–7. SPIE (2017)
29. Yousefi, B., Sfarra S., S.F., Maldague, X.P.: Irndt inspection via sparse principal component thermography. In: Electrical and Computer Engineering (CCECE), 2017 IEEE 30th Canadian Conference on, pp. 1–4. IEEE (2018)
30. Yousefi, B., Sharifipour, H.M., Castanedo, C.I., Maldague, X.P.: Automatic irndt inspection applying sparse pca-based clustering. In: Electrical and Computer Engineering (CCECE), 2017 IEEE 30th Canadian Conference on, pp. 1–4. IEEE (2017)
31. Yousefi, B., Sojasi, S., Castanedo, C.I., Beaudoin, G., Huot, F., Maldague, X.P., Chamberland, M., Lalonde, E.: Mineral identification in hyperspectral imaging using sparse-pca. In: Thermosense: Thermal Infrared Applications XXXVIII, vol. 9861, p. 986118. International Society for Optics and Photonics (2016)

32. Yousefi, B., Sojasi, S., Castanedo, C.I., Maldague, X.P., Beaudoin, G., Chamberland, M.: Comparison assessment of low rank sparse-pca based-clustering/classification for automatic mineral identification in long wave infrared hyperspectral imagery. Infrared Physics & Technology **93**, 103–111 (2018)
33. YOUSEFI, B., SOJASI, S., CASTANEDO, C.I., MALDAGUE, X.P., BEAUDOIN, G., CHAMBERLAND, M.: Continuum removal for ground based lwir hyperspectral infrared imagery applying non-negative matrix factorization (2018)
34. Zhang, H., Hassler, U., Genest, M., Fernandes, H., Robitaille, F., Ibarra-Castanedo, C., Joncas, S., Maldague, X.: Comparative study on submillimeter flaws in stitched t-joint carbon fiber reinforced polymer by infrared thermography, microcomputed tomography, ultrasonic c-scan and microscopic inspection. Optical Engineering **54**(10), 104,109–104,109 (2015)
35. Zhang, H., Robitaille, F., Grosse, C.U., Ibarra-Castanedo, C., Martins, J.O., Sfarra, S., Maldague, X.P.: Optical excitation thermography for twill/plain weaves and stitched fabric dry carbon fibre preform inspection. Composites Part A: Applied Science and Manufacturing (2018)
36. Zhang, H., Sfarra, S., Sarasini, F., Ibarra-Castanedo, C., Perilli, S., Fernandes, H., Duan, Y., Peeters, J., Avelidis, N.P., Maldague, X.: Optical and mechanical excitation thermography for impact response in basalt-carbon hybrid fiber-reinforced composite laminates. IEEE Transactions on Industrial Informatics (2017)